Toward a Direct Measure of the Galactic Acceleration

Sukanya Chakrabarti[1,12] , Jason Wright[2] , Philip Chang[3] , Alice Quillen[4] , Peter Craig[1], Joey Territo[1], Elena D'Onghia[5],
Kathryn V. Johnston[6,11], Robert J. De Rosa[7], Daniel Huber[8] , Katherine L. Rhode[9] , and Eric Nielsen[10]

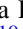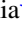[1] School of Physics and Astronomy, Rochester Institute of Technology, 84 Lomb Memorial Drive, Rochester, NY 14623, USA; chakrabarti@astro.rit.edu
[2] Department of Astronomy & Astrophysics, Center for Exoplanets and Habitable Worlds, and Penn State Extraterrestrial Intelligence Center, 525 Davey Laboratory,
The Pennsylvania State University, University Park, PA 16802, USA
[3] Department of Physics, University of Wisconsin–Milwaukee, 3135 North Maryland Avenue, Milwaukee, WI 53211, USA
[4] Department of Physics and Astronomy, University of Rochester, Rochester, NY, USA
[5] Department of Astronomy, University of Wisconsin–Madison, Madison, WI, USA
[6] Department of Astronomy, Columbia University, New York, NY, USA
[7] European Southern Observatory, Alonso de Córdova 3107, Vitacura, Santiago, Chile
[8] University of Hawaii, Honolulu, HI, USA
[9] Department of Astronomy, Indiana University, Bloomington, IN 47405, USA
[10] Stanford University, Stanford, CA, USA
[11] Center for Computational Astrophysics, Flatiron Institute, New York, NY, USA
[12] Institute for Advanced Study, 1 Einstein Drive, Princeton, NJ 08540 USA

Abstract

High-precision spectrographs can enable not only the discovery of exoplanets, but can also provide a fundamental measurement in Galactic dynamics. Over about 10 year baselines, the expected change in the line-of-sight velocity due to the Galaxy's gravitational field for stars at ~kiloparsec scale distances above the Galactic midplane is ~few tens of cm s^{-1}, and may be detectable by the current generation of high-precision spectrographs. Here, we provide theoretical expectations for this measurement based on both static models of the Milky Way and isolated Milky Way simulations, as well from controlled dynamical simulations of the Milky Way interacting with dwarf galaxies. We simulate a population synthesis model to analyze the contribution of planets and binaries to the Galactic acceleration signal. We find that while low-mass, long-period planetary companions are a contaminant to the Galactic acceleration signal, their contribution is very small. Our analysis of ~10 years of data from the Lick–Carnegie Exoplanet Survey HIRES/Keck precision radial-velocity (RV) survey shows that slopes of the RV curves of standard RV stars agree with expectations of the local Galactic acceleration near the Sun within the errors, and that the error in the slope scales inversely as the square root of the number of observations. Thus, we demonstrate that a survey of stars with low intrinsic stellar jitter at kiloparsec distances above the Galactic midplane for realistic sample sizes can enable a direct determination of the dark matter density.

Unified Astronomy Thesaurus concepts: Dark matter (353); Dark matter density (354); Exoplanets (498); Exoplanet astronomy (486); Milky Way Galaxy (1054)

1. Introduction

High-precision spectrographs have recently come online that are designed to search for Earth-sized planets orbiting Sun-like stars and are expected to have an instrumental precision of order 10 cm s^{-1} (Pepe et al. 2010; Fischer et al. 2016; Wright & Robertson 2017). The NEID spectrograph has been designed to have an instrumental precision of 30 cm s^{-1}, and was deployed last year on the WIYN 3.5m telescope (Schwab et al. 2016). The Very Large Telescope's ESPRESSO has demonstrated precision better than 30 cm s^{-1} for quiet stars (Pepe et al. 2020). Additionally, next-generation Doppler spectrographs on 10m+ telescopes such as the Keck Planet Finder (Gibson et al. 2016) will push such exquisite radial-velocity (RV) precision to fainter stars and larger distances. These spectrographs can also be used to directly measure the Galactic acceleration, which gives a constraint on the dark matter density. As such, it is likely the most fundamental measurement that can be made in Galactic dynamics.

To determine the nature of the dark matter particle from direct dark matter detection experiments requires an independent measure of the local dark matter density (Read 2014), as extrapolated to the lab. The traditional method is to estimate the acceleration using stellar kinematics, and accounting for the baryon budget in the solar neighborhood, infer the total density from the Jeans analysis (which assumes equilibrium) using stellar velocity dispersions (Kuijken & Gilmore 1989; Holmberg & Flynn 2000; McKee et al. 2015; Widmark & Monari 2019). Other kinematical estimates besides the Jeans analysis have also been explored (Salucci et al. 2010). In regions far from the Galactic midplane where baryonic processes do not affect halo shapes (Prada et al. 2019), the dark matter density may constrain the shape of the Milky Way's dark matter halo (Read 2014), and how it is affected by cosmological accretion and satellite interactions via a study of its substructure. This work is largely focused on measurements at a few kiloparsec distances above the Galactic midplane. A measurement of the Galactic acceleration would allow us to determine the viability of different dark matter models, as well as others including modified Newtonian gravity (Milgrom 1983, 2010), and toward understanding the history of cosmic accretion in the Milky Way.

Recent work has shown that there are significant differences between the *true* density measured in a simulation and the density inferred from using the Jeans approximation, especially in regions where the Galaxy is perturbed (Haines et al. 2019). Analysis of Gaia DR-2 data has revealed the so-called phase-space spiral (Antoja et al. 2018), as well as the Enceladus

merger (Helmi et al. 2018), clearly indicating a Galaxy that is out of equilibrium.

Earlier work (Quercellini et al. 2008; Ravi et al. 2019; Silverwood & Easther 2019) estimates that over a baseline of about 10 years, high-precision spectrographs should be able to directly measure the local acceleration of the Galaxy, i.e., relative to the solar acceleration. The advent of high-resolution spectrographs, coupled with a better understanding of stellar jitter (Yu et al. 2018; Luhn et al. 2020a), now renders this fundamental measurement feasible. Gaia's proper motion data will not have sufficient accuracy to detect the Galactic acceleration, even over 10 year baselines (Silverwood & Easther 2019). Here, we show that targeted surveys with high-precision spectrographs are a promising route that can deliver this measurement.

In this Letter, we go beyond earlier work by laying out theoretical expectations from not only static models of the Milky Way, but also from dynamically evolving simulations of the Milky Way (Section 2) interacting with dwarf galaxies, and contrast the differences with static and isolated high-resolution models of the Galaxy that include the effect of the Galactic bar. In Section 3, we simulate a Galactic population composed of single stars, binaries, and planets, and thereby calculate the effect of contaminants (stellar binaries and planets) on the Galactic acceleration. We analyze existing 10 year data from the Lick–Carnegie Exoplanet Survey (LCES) High Resolution Echelle Spectrometer (HIRES)/Keck precision radial-velocity exoplanet survey of stars near the Sun for standard RV stars. We show that the errors in the slopes of the RV curves, although non-Gaussian (arising from stellar jitter and instrumental noise), may be taken to be Gaussian for the purposes of quantifying the effect of this noise on the measured acceleration. One of the significant advances of this work is that we show that (Section 3) the contamination to the Galactic signal from planets in a realistic sample size is very small. We conclude in Section 4.

2. Theoretical Expectations

2.1. Static and Isolated Milky Way Models

For a baseline expectation for the local Galactic acceleration, we begin by considering static models of the Milky Way. The radial acceleration is $\sim v_c^2/R_\odot$, where v_c is the circular velocity of the Sun and $R_\odot$ is the Galactocentric radius of the Sun. The GRAVITY Collaboration et al. (2018) have measured $R_\odot$ to high precision, and this measurement, combined with the tangential component of the solar peculiar motion, gives us v_c. Thus, we have reasonably good bounds on the radial acceleration. It will be useful to verify the direct acceleration method as compared to current constraints on the radial acceleration near the Sun; Silverwood & Easther (2019) have discussed the range of radial accelerations for a specific Milky Way potential model, which give $\sim$a few cm s^{-1} near the Sun. Here, we focus on the vertical acceleration that is significantly more uncertain at $\sim$kiloparsec distances above the Galactic midplane.

To illustrate the range of possible vertical accelerations, we consider a range for the Milky Way total mass that spans $\sim 1-2 \times 10^{12} M_\odot$, as found in the literature (Boylan-Kolchin et al. 2013; Piffl et al. 2014; Fritz et al. 2018; Deason et al. 2019; Posti & Helmi 2019; Watkins et al. 2019). Figure 1 depicts the change in the line-of-sight velocity in the vertical
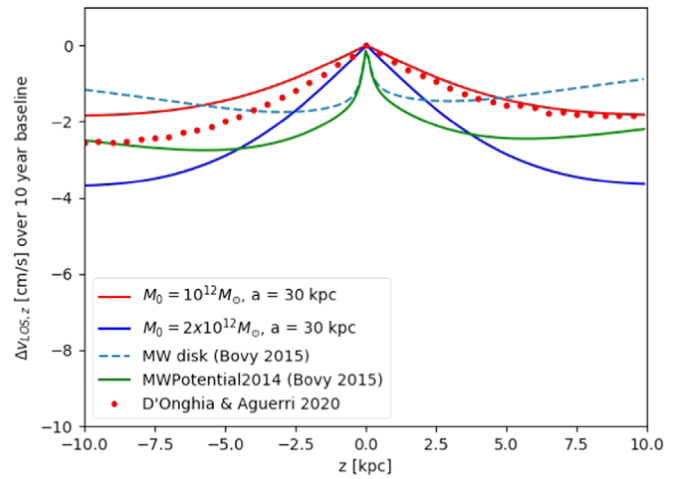

Figure 1. Change in the line-of-sight velocity over a baseline of 10 years in a Galaxy model with a dark matter halo having a Hernquist profile and a total mass of $2 \times 10^{12} M_\odot$ (blue line) and $10^{12} M_\odot$ (red line), both with a scale length = 30 kpc. Also shown is the contribution from Bovy's (2015) Milky Way disk model (dashed blue line), and the MWPotential2014 potential (green line), and a recent high-resolution isolated simulation of the Milky Way (D'Onghia & Aguerri 2020; in red dots). RV observations at $\sim$kiloparsec distances off the midplane near the Sun would produce measurable changes in the line-of-sight velocity, and would primarily probe the dark matter component of the potential.

direction ($\Delta v_{\mathrm{LOS},z}$) for stars in a Galaxy model that incorporates a dark matter halo having a Hernquist (1990) density profile, shown here for masses of $10^{12} M_\odot$ (solid red line) and $2 \times 10^{12} M_\odot$ (solid blue line), both with a scale length of 30 kpc. Here, we have used the Galpy[13] software (Bovy 2015) to calculate the line-of-sight acceleration for a specified potential, relative to the Sun's acceleration. We take the Sun's position to be at Galactocentric coordinates X = 8.1 kpc, Y = 0, Z = 0.05 pc. The line of sight is taken to be from the Sun to some vertical height above or below the Sun. The change in the line-of-sight velocity is shown here over a time baseline of ten years. Also shown here is the contribution from the Milky Way disk model (dashed blue line) developed by Bovy (2015), and for the MWPotential2014 model for the total Milky Way potential as described in Bovy (2015). $\Delta v_{\mathrm{LOS},z}$ is negative and $\sim$a few tens of cm s^{-1} for $z \geqslant 2$ kpc off the Galactic midplane, at which point the potential is clearly dominated by the dark matter halo.

Estimates of the acceleration using observations of the vertical kinematics and density of A and F stars in the context of the vertical Jeans equation (Holmberg & Flynn 2000) at 1 kpc above the midplane give a $\Delta v_{LOS,z}$ of 1 cm s^{-1}, which is consistent with the range shown here.

An important consideration for isolated models of the Milky Way is the effect of the bar on the Galaxy. A recent high-resolution N-body simulation of the Milky Way (D'Onghia & Aguerri 2020) adopts a long-bar scenario (extending about 5 kpc from the Galactic center), which reproduces the formation of the Hercules stream, as well as other features in the solar vicinity. Figure 1 also depicts a comparison to this simulation of the Milky Way (shown here in red dots). Here, the Sun is placed at Galactocentric coordinates X = 7.15, Y = −3.8 kpc, following their work, and we compute the acceleration above and below the midplane from the Sun. For this and the

---
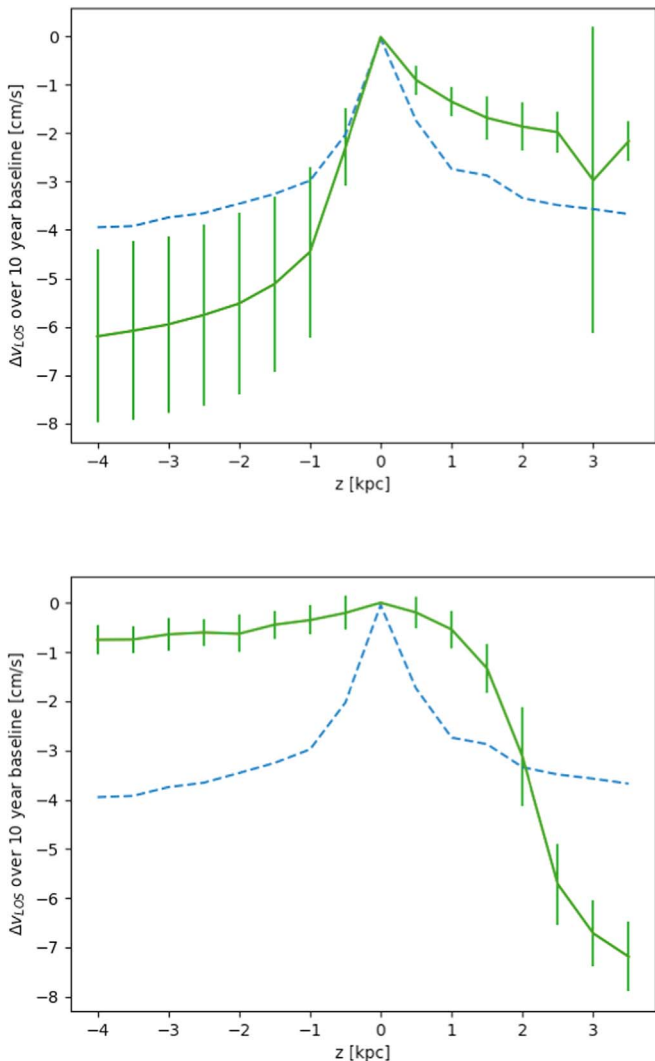
[13] http://github.com/jobovy/galpy

Figure 2. (a) Change in the line-of-sight velocity for a simulation of Milky Way interacting with the Antlia 2 dwarf galaxy at present day (solid line) and at early times prior to the interaction with Antlia 2 (dashed line) (Chakrabarti et al. 2019); solid line shows the average over a ring of radius $r = 8$ kpc, and the error bars show the standard deviation along the azimuth. (b) $\Delta v_{LOS,z}$ for the interaction of the Sagittarius dwarf galaxy with the Milky Way (Chakrabarti et al. 2019), with the dashed line displaying the acceleration profile at early times, and the solid line corresponding to the present day.

smoothed particle hydrodynamics (SPH) simulations that we analyze below, we compute the acceleration directly from the particle information. As is clear, the effect of spiral arms and the bar do not lead to a pronounced asymmetry in the vertical acceleration, and the magnitude of the acceleration is comparable to the static cases shown.

2.2. Simulations of the Milky Way Interacting with Dwarf Galaxies

The Milky Way exhibits a plethora of signatures of interactions, including tidal streams such as that of the Sagittarius (Sgr) dwarf galaxy (Ibata et al. 1994), a warp and large planar disturbances in the HI disk (Levine et al. 2006), vertical waves in the stellar disk (Xu et al. 2015), as well as more recent discoveries from Gaia DR-2 including the Gaia Enceladus merger (Helmi et al. 2018). Thus, it is important to

consider a dynamically evolving galaxy undergoing external perturbations, and its effect on the Galactic acceleration.

Figure 2 depicts $\Delta v_{LOS,z}$ over a time baseline of 10 years for the simulation of the Antlia 2 dwarf interacting with the Milky Way, and a simulation of the Sgr dwarf interaction (as described in Chakrabarti et al. 2019). Both simulations use observationally realistic orbits derived from the Gaia proper motions. The simulations are initialized with a more massive dark matter halo relative to D'Onghia & Aguerri (2020), by about a factor of 2. The present-day acceleration profile is shown in the solid lines, and the acceleration profile at early times (prior to the interaction with the dwarf galaxy) is shown in the dashed line. The simulation of the Antlia 2 dwarf reproduces the observed planar HI disturbances in the outer disk (Levine et al. 2006). The Antlia 2 dwarf galaxy radial location is close to that of a predicted dwarf galaxy (Chakrabarti & Blitz 2009) that recently perturbed our Galaxy. While these simulations of Milky Way–like galaxies recover aspects of the observed Galaxy, such as the observed HI disturbances (Chakrabarti & Blitz 2009, 2011), and large-scale properties of moving groups in the Galactic disk (Craig et al. 2019), we do not resolve the solar neighborhood. Therefore, we take the Sun to be along a ring of radius $r = 8.1$ kpc, and calculate the acceleration along vertical lines of sight at various azimuths. The solid line shows the average value of $\Delta v_{LOS,z}$, and the errors show the standard deviation. In contrast to the models shown in Figure 1, both these simulations show a clear asymmetry in the acceleration profile, particularly for $|z| > 1$ kpc relative to the Galactic midplane. Moreover, the acceleration profile develops this asymmetry following the interaction, as is clear from comparing the early-time (i.e., prior to the interaction) acceleration profile (shown in the dashed lines) with the present-day acceleration profile, where the latter is distinctly more asymmetric.

It is not surprising that the Sgr dwarf interaction shows a more prominent vertical asymmetry, as it is on a polar orbit, relative to the Antlia 2 interaction. The Antlia 2 dwarf galaxy is on a nearly coplanar orbit and excites large planar disturbances in the Galactic disk, leading to a larger standard deviation at various azimuths, compared to the Sgr interaction where the variation along the azimuth is smaller. An observed asymmetry in the acceleration profile may be the signature of a perturbing dwarf galaxy. The effects of multiple perturbers in cosmological simulations may lead to more complex vertical acceleration profiles.

3. Effects of Contaminants

In order to detect the Galactic acceleration, we have to carefully select our sample of stars. We select cool stars with low radial-velocity "jitter" (e.g. Wright 2005), such that with repeated N measurements, one may expect to improve our precision by $1/\sqrt{N}$ to the level of $10 \, \mathrm{cm \, s^{-1}}$. Specifically, we select stars from Gaia DR-2 (Gaia Collaboration et al. 2018) that are expected to have low RV jitter on the basis of their stellar parameters (Yu et al. 2018) and their Gaia colors, which recent work has shown can be translated to an empirical constraint on the stellar jitter (Luhn et al. 2020b). As discussed in Luhn et al. (2020b), the metric ΔG corresponds to evolved stars that correlate with low stellar jitter (for $\Delta G < 1.4$), which can be identified from their Gaia colors, and distance from the main sequence. We choose slightly evolved subgiants as a compromise between selecting stars at the "jitter minimum"
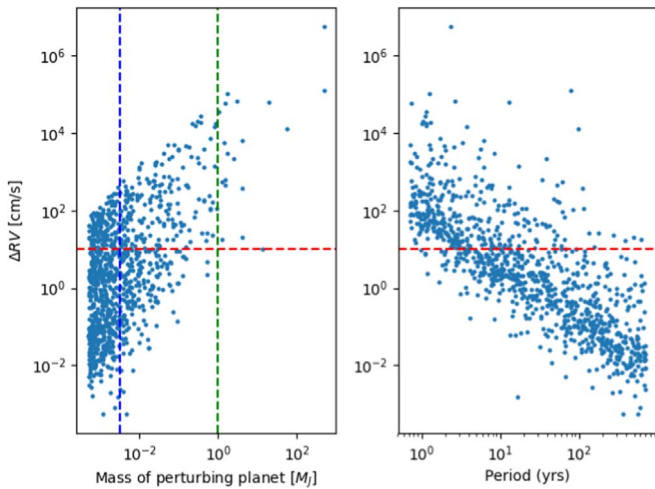
Figure 3. Δv_{LOS} over a time baseline of 10 years (a) as a function of the perturbing planet mass, and (b) as a function of the period, shown for circular Keplerian orbits. The red horizontal line marks $\Delta RV = 10 \text{ cm s}^{-1}$, and the dashed blue and green vertical lines mark Earth- and Jupiter-mass planets, respectively.

Figure 4. Top panel: histogram of ΔRV over a 10 year baseline in a population of single stars, stars with planets on circular Keplerian orbits, and stellar binaries, color-coded by the object type (single stars, stars with planets, binaries). The inset shows a zoom-in centered on the mean of the single star's ΔRV, and out to $\pm 5\sigma$ from the mean.

and intrinsically bright stars observable at high RV precision at kiloparsec distances. In addition to stellar jitter, another contaminant is RV variations due to planetary companions and stellar binaries. Below, we consider in turn the contribution from planetary companions, stellar binaries, and stellar jitter and instrumental noise to the Galactic signal.

3.1. Planets and Binaries

Figure 3 shows ΔRV as a function of the perturbing planet mass (left panel) and period of orbit (right panel), for 1000 realizations. This is the parent population of planets that we draw from in constructing the synthetic population we have simulated. Here, we have considered circular Keplerian orbits with random inclination and phase, with a distribution for the semimajor axis a that follows $\log \Delta a/a = \text{constant}$ (in the range of 1–100 au), motivated by observations (Nielsen et al. 2019), and a planet mass distribution that follows m_p^{-2}, where m_p is the planet mass (in the range of Mercury mass to 500 Jupiter masses).

We have calculated accelerations instantaneously, which is a poor approximation for short-period (<10 year) periods but, only the long-period (>10 year), low-mass ($10^{-2} M_J$) planets contribute to the regime where one would make the Galactic acceleration measurement, i.e., for $\Delta RV \sim 10 \text{ cm s}^{-1}$. As we find below, the relative fraction of this contaminant to the Galactic signal is very small. Furthermore, with continuous monitoring, short-period systems can be identified and culled from the sample. The stellar binary population is similarly drawn from distributions outlined in Stonkutė et al. (2018) for subgiants, assuming circular Keplerian orbits with random inclination and phase; for simplicity we assume the binaries have masses of 1 and 2 solar masses.

To analyze the contribution of planets and binaries to the Galactic acceleration signal, we create a synthetic population composed of single stars that probe the Galactic acceleration, stellar binaries, and stars with planetary companions, adopting observed fractions of stellar binaries for subgiants ($\sim 30\%$; Stonkutė et al. 2018), and planet occurrence rate ($\sim 7\%$; Nielsen et al. 2019). There is at present no survey that fully
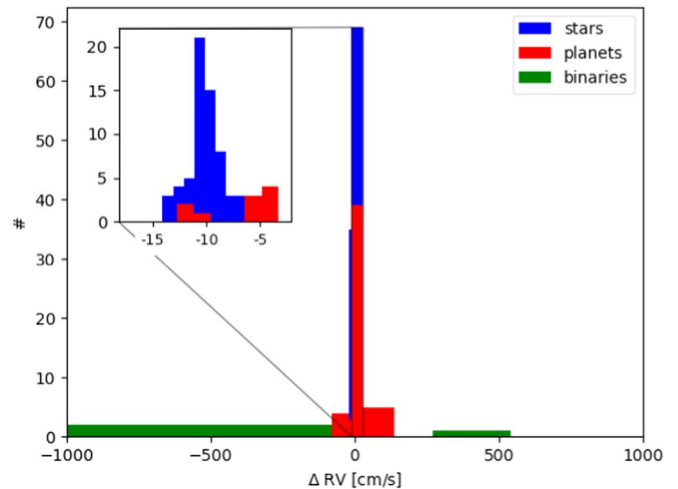
encompasses the range of period, semimajor axis, and planet mass that we are interested in. Therefore, our results are based on an extrapolation of presently observed planet demographics, which mainly probes the high-mass end of the planet distribution around subgiant stars. We choose a normalization for the planet mass distribution that ensures that observed planet demographics are reproduced (by assumption, 50% of the stars in our synthetic population are assigned three planetary companions following the distributions above, which leads to a mean number of about two planets per star). This typically leads to a few percent of the population having massive planetary companions (with masses between Jupiter mass to 20 times the Jupiter mass and a semimajor axis between 10–100 au), which is consistent with the 1σ range of the observed massive planet occurrence rate fraction for subgiants (Nielsen et al. 2019).

To whittle the sample of observable stars down to cool, low-jitter stars with metallicity close to solar (such that current instruments can achieve RV precision $\sim 1 \text{ m s}^{-1}$) at kiloparsec distances that are observable by current-generation instruments to high RV precision, we take the following cuts in height ($|z| > 2$ kpc), temperature ($T_{\text{eff}} < 6600 \text{ K}$), ΔG ($1.5 > \Delta G > 0.14$), and magnitude (G mag < 15), from Gaia DR-2, which leaves a total number of 124 stars, when we consider a metallicity fraction ($\sim 15\%$) of halo stars (Conroy et al. 2019) of $[\text{Fe}/\text{H}] > -0.5$. For simplicity, here we take the Galactic acceleration signal to be a Gaussian, with a mean value equal to the expected signal at a vertical height of ~ 3 kpc ($-3.18 \times 10^{-8} \text{ cm s}^{-2}$), and a standard deviation equal to 30% of this value.

Figure 4 displays the resultant histogram of ΔRV from such a nonhomogeneous population, for single stars, stellar binaries, and stars with planets. To display the contribution from planets to the Galactic signal, the inset shows a zoom-in centered close to the mean of the single stars' ΔRV within $\pm 5\sigma$ of the mean, while the larger figure has wider bins to display the full population. Binaries (shown in green) have large ΔRV (Stonkutė et al. 2018), and thus they separate out from the planet and the Galactic acceleration signal from single stars, and therefore would be easily discarded. Although stars with

long-period, low-mass planets are a contaminant to the Galactic acceleration, their contribution, as shown in the inset, is a small fraction of the signal from single stars (typically about 3% within 3σ). The exact contribution varies from realization to realization due to Poisson noise. Converting from ΔRV to accelerations (over a 10 year baseline) gives for a typical realization a mean acceleration for single stars of $-3.1 \times 10^{-8}\,\mathrm{cm\,s^{-2}}$, with a standard deviation of $6.6 \times 10^{-9}\,\mathrm{cm\,s^{-2}}$. The mean acceleration of all stars (including the stars with planets) that fall within $\pm 5\sigma$ of the mean of the single stars is $-3.12 \times 10^{-8}\,\mathrm{cm\,s^{-2}}$, with a 1σ of $7.87 \times 10^{-9}\,\mathrm{cm\,s^{-2}}$. The p-value from the Kolmogorov–Smirnov test for the two distributions corresponding to all stars that fall within $\pm 5\sigma$ of the mean of the single stars and stars with planets that fall in this range is consistently $\sim 10^{-4}$ or lower, indicating that these two distributions are clearly distinct. Thus, we can reject the null hypothesis that the signal is due to stars with planetary companions at high confidence. The mean acceleration experienced by standard RV stars is much less than the mean acceleration for the planet population, which is due to the fact that the majority of stars with planets have at least one with a large acceleration.

3.2. Sources of Noise in RV Data: The LCES HIRES/Keck Precision Radial-velocity Exoplanet Survey

Observational data will be affected by both stellar "jitter" that arises from intrinsic stellar variability, including stellar oscillations, granulation, short-term activity from stellar rotation, and long-term activity due to magnetic fields (Yu et al. 2018), as well as instrumental noise. The expected contribution to RV jitter for subgiants on a day-to-month timescale from oscillations and granulation is $\sim 1.5\,\mathrm{m\,s^{-1}}$ (Yu et al. 2018). These sources of noise (stellar jitter and instrumental noise) are non-Gaussian. An existing long-term (more than a decade) RV data set of stars near the Sun was produced by the LCES Team, using radial velocities from HIRES on Keck, and is described in Butler et al. (2017). To determine if we may model observational sources of noise as being effectively Gaussian for the purposes of the acceleration measurement, we select standard RV stars from the data from Butler et al. (2017), and calculate the error in the slope of the RV curve. We only consider data from 2004 June onward to avoid the discontinuity in the data, which still yields nearly 10 years of RV data. The typical RV precision of this data set is $\sim 1\,\mathrm{m\,s^{-1}}$.

Figure 5 shows the error in the RV slope for 18 standard RV stars as we select smaller samples of the total observational sample for a given star (removing every nth observation, from $n = 2$, up to half the observations, while holding the baseline constant). As is clear, except for small sample sizes (<20), the error in the slope scales as $1/\sqrt{(N)}$, where N is the sample size. Therefore, we may reasonably expect that N-independent observations of the same star will serve to effectively increase the RV precision of observations as $1/\sqrt{N}$. For a long-term monitoring survey, one may then carry out individual RV measurements at some threshold precision, for example, $\sim 1\,\mathrm{m\,s^{-1}}$ RV precision for individual measurements, and thus measure the acceleration with precisions approaching $\sim 10\,\mathrm{cm\,s^{-1}}$ over a baseline of 10 years from 100 independent measurements. There are hopes and expectations that the problem of RV jitter can be mitigated or solved and that the measurement uncertainty of center-of-mass motions of stars
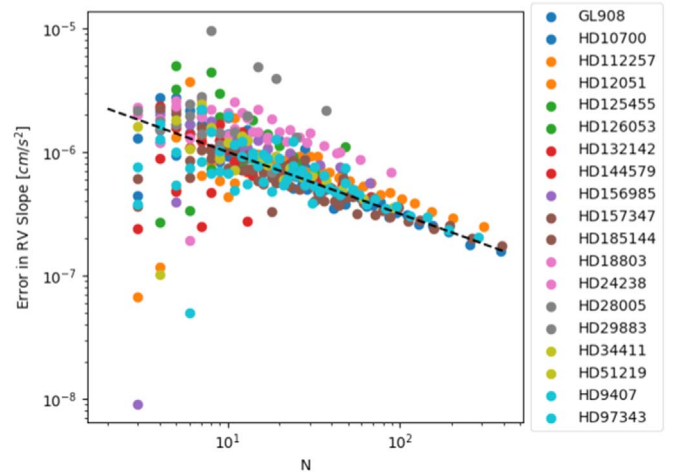

Figure 5. Error in the RV slope for the LCES/HIRES Keck observations as a function of sample size, N, for standard RV stars from Butler et al. (2017). Each star is color-coded and labeled in the legend. Overlaid is a dashed line that varies as $N^{-1/2}$, where N is the number of observations.

can be reduced toward the instrumental precision, further improving the precision of the acceleration measurements. These methods will rely on simultaneously measured activity indices, which are collected as part of the measurement (e.g., Ca lines).

The average slope of the RV curve for this sample of 18 standard RV stars is $-5.2 \times 10^{-8}\,\mathrm{cm\,s^{-2}} \pm 7 + 10^{-7}\,\mathrm{cm\,s^{-2}}$. Due to the large error here, we cannot determine the local Galactic acceleration accurately, but the average value is nevertheless consistent within the errors with expectations of the local Galactic acceleration based on models for stars within a few hundred parsecs of the Sun.

4. Conclusions

We have analyzed the vertical acceleration experienced by stars in the Galaxy in the context of a number of different models of the Milky Way: static models, isolated high-resolution simulations, and simulations that include interactions between the Milky Way and dwarf galaxies. The magnitude of the change in the line-of-sight velocity over 10 year baselines is $\sim$a few tens of $\mathrm{cm\,s^{-1}}$ at kiloparsec distances off the Galactic midplane in static models (with a significant dependence on the mass of the dark matter halo), and in isolated simulations. Simulations of the Milky Way interacting with dwarf galaxies have distinctly asymmetric vertical accelerations, in particular for $|z| > 1$ kpc relative to the Galactic midplane. We find that although low-mass ($<10^{-2}$ M_{Jupiter}), long-period (>10 yr) planets are a contaminant, they do not overwhelm the Galactic acceleration signal in a realistic sample size of stars selected from Gaia DR-2 that are currently observable. We find that one can reject the null hypothesis that the signal is due to stars with planetary companions at high confidence.

We have analyzed 10 year data of standard RV stars from the LCES HIRES/Keck precision radial-velocity survey. Although the error in the RV slope is non-Gaussian, we find that we may consider it to be effectively Gaussian for the purposes of the Galactic acceleration measurement, as long as a sufficient number of epochs are obtained ($N > 20$). High-precision RV measurements at kiloparsec distances will enable us to determine the total density directly from the Poisson equation, and the dark matter density given an accounting of the baryon

budget; they will also provide a direct view of dark matter substructure in the Milky Way.

Analyzing cosmological simulations with both cold dark matter models as well as alternatives to cold dark matter, such as self-interacting dark matter (Spergel & Steinhardt 2000; Tulin & Yu 2018), will help us understand if the nature of the dark matter particle produces measurable differences at these scales. Determining the Galactic acceleration lies at the nexus of three areas that are often disparate—dark matter detection, studies of planet demographics, and Galactic dynamics, and can potentially produce discoveries in all three areas.

ORCID iDs

Sukanya Chakrabarti ⓘ https://orcid.org/0000-0001-6711-8140
Jason Wright ⓘ https://orcid.org/0000-0001-6160-5888
Philip Chang ⓘ https://orcid.org/0000-0002-2137-2837
Alice Quillen ⓘ https://orcid.org/0000-0003-1280-2054
Daniel Huber ⓘ https://orcid.org/0000-0001-8832-4488
Katherine L. Rhode ⓘ https://orcid.org/0000-0001-8283-4591
Eric Nielsen ⓘ https://orcid.org/0000-0001-6975-9056

References

Antoja, T., Helmi, A., Romero-Gómez, M., et al. 2018, Natur, 561, 360
Bovy, J. 2015, ApJS, 216, 29
Boylan-Kolchin, M., Bullock, J. S., Sohn, S. T., Besla, G., & van der Marel, R. P. 2013, ApJ, 768, 140
Butler, R. P., Vogt, S. S., Laughlin, G., et al. 2017, AJ, 153, 208
Chakrabarti, S., & Blitz, L. 2009, MNRAS, 399, L118
Chakrabarti, S., & Blitz, L. 2011, ApJ, 731, 40
Chakrabarti, S., Chang, P., Price-Whelan, A. M., et al. 2019, ApJ, 886, 67
Conroy, C., Naidu, R. P., Zaritsky, D., et al. 2019, ApJ, 887, 237
Craig, P., Chakraborti, S., Newberg, H. J., & Quillen, A. 2019, arXiv:1911.01392
D'Onghia, E. L., & Aguerri, J. A. 2020, ApJ, 890, 117
Deason, A. J., Belokurov, V., & Sanders, J. L. 2019, MNRAS, 490, 3426
Fischer, D. A., Anglada-Escude, G., Arriagada, P., et al. 2016, PASP, 128, 066001
Fritz, T. K., Battaglia, G., Pawlowski, M. S., et al. 2018, A&A, 619, A103
Gaia Collaboration, Brown, A. G. A., & Vallenari, A. 2018, A&A, 616, A1
Gibson, S. R., Howard, A. W., Marcy, G. W., et al. 2016, Proc. SPIE, 9908, 990870
GRAVITY Collaboration, Abuter, R., Amorim, A., et al. 2018, A&A, 615, L15
Haines, T., D'Onghia, E., Famaey, B., Laporte, C., & Hernquist, L. 2019, ApJL, 879, L15
Helmi, A., Babusiaux, C., Koppelman, H. H., et al. 2018, Natur, 563, 85
Hernquist, L. 1990, ApJ, 356, 359
Holmberg, J., & Flynn, C. 2000, MNRAS, 313, 209
Ibata, R. A., Gilmore, G., & Irwin, M. J. 1994, Natur, 370, 194
Kuijken, K., & Gilmore, G. 1989, MNRAS, 239, 651
Levine, E. S., Blitz, L., & Heiles, C. 2006, ApJ, 643, 881
Luhn, J. K., Wright, J. T., Howard, A. W., & Isaacson, H. 2020a, AJ, 159, 235
Luhn, J. K., Wright, J. T., & Isaacson, H. 2020b, AJ, 159, 236
McKee, C. F., Parravano, A., & Hollenbach, D. J. 2015, ApJ, 814, 13
Milgrom, M. 1983, ApJ, 270, 365
Milgrom, M. 2010, MNRAS, 403, 886
Nielsen, E. L., De Rosa, R. J., Macintosh, B., et al. 2019, AJ, 158, 13
Pepe, F., Cristiani, S., Rebolo, R., et al. 2020, arXiv:2010.00316
Pepe, F. A., Cristiani, S., Rebolo Lopez, R., et al. 2010, Proc. SPIE, 7735, 77350F
Piffl, T., Binney, J., McMillan, P. J., et al. 2014, MNRAS, 445, 3133
Posti, L., & Helmi, A. 2019, A&A, 621, A56
Prada, J., Forero-Romero, J. E., Grand, R. J. J., Pakmor, R., & Springel, V. 2019, MNRAS, 490, 4877
Quercellini, C., Amendola, L., & Balbi, A. 2008, MNRAS, 391, 1308
Ravi, A., Langellier, N., Phillips, D. F., et al. 2019, PhRvL, 123, 091101
Read, J. I. 2014, JPhG, 41, 063101
Salucci, P., Nesti, F., Gentile, G., & Frigerio Martins, C. 2010, A&A, 523, A83
Schwab, C., Rakich, A., Gong, Q., et al. 2016, Proc. SPIE, 9908, 99087H
Silverwood, H., & Easther, R. 2019, PASA, 36, e038
Spergel, D. N., & Steinhardt, P. J. 2000, PhRvL, 84, 3760
Stonkutė, E., Church, R. P., Feltzing, S., & Johnson, J. A. 2018, arXiv:1804.09189
Tulin, S., & Yu, H.-B. 2018, PhR, 730, 1
Watkins, L. L., van der Marel, R. P., Sohn, S. T., & Evans, N. W. 2019, ApJ, 873, 118
Widmark, A., & Monari, G. 2019, MNRAS, 482, 262
Wright, J. T. 2005, PASP, 117, 657
Wright, J. T., & Robertson, P. 2017, RNAAS, 1, 51
Xu, Y., Newberg, H. J., Carlin, J. L., et al. 2015, ApJ, 801, 105
Yu, J., Huber, D., Bedding, T. R., & Stello, D. 2018, MNRAS, 480, L48